Dissipative Particle Dynamics via Molecular Dynamics

Karl P. Travis

Immobilisation Science Laboratory, Department of Materials Science and Engineering
University of Sheffield, Sheffield, S1 3JD, UK
E-mail: k.travis@sheffield.ac.uk

Abstract: We demonstrate that the main features of DPD may be obtained using molecular dynamics employing a deterministic thermostat. This apparent isomorphism holds as long as the MD pair potentials are sufficiently smooth and short ranged, which gives rise to a quadratic equation of state (pressure as a function of density). This is advantageous because it avoids the need to use stochastic forces, enabling a wider choice of integration algorithms, involves fully time reversible motion equations and offers a simpler algorithm to achieve the same objective. The isomorphism is explored and shown to hold in 2 and 3 physical dimensions as well as for binary and ternary systems for two different choices of pair potential. The mapping between DPD and Hildebrand's regular solution theory (a consequence of the quadratic equation of state) is extended to multicomponent mixtures. The procedure for parametrization of MD (identical to that of DPD) is outlined and illustrated for a equimolar binary mixture of SnI_4 and isooctane (2,2,4-trimethylpentane).
Key words: dissipative particle dynamics, phase equilibria, molecular dynamics

I. INTRODUCTION

Dissipative Particle Dynamics (DPD) is a particle-based simulation method developed in the 1990s by Hoogerbrugge and Koelman [1], sharing features of both molecular dynamics and lattice gas automata. DPD rapidly gained popularity within the simulation community following developments and improvements to the basic algorithm by Español and Warren [2], Groot and Warren [3], and others.

In DPD, the total force acting on a particle is given by the sum of three types of pairwise additive forces – conservative, dissipative and random:

$$\mathbf{F}_i^{tot} = \sum_{j \neq i} \mathbf{F}_{ij}^C + \mathbf{F}_{ij}^D + \mathbf{F}_{ij}^R \tag{1}$$

Pairwise additivity ensures momentum conservation, a necessary condition for hydrodynamic behaviour. The three types of force are respectively given by

$$\mathbf{F}_{ij}^C = a_{ij} w^C (r_{ij}) \widehat{\mathbf{r}}_{ij} \tag{2}$$

$$\mathbf{F}_{ij}^D = -\gamma w^D (r_{ij}) (\mathbf{r}_{ij} \cdot \mathbf{v}_{ij}) \widehat{\mathbf{r}}_{ij} \tag{3}$$

$$\mathbf{F}_{ij}^R = \sigma w^R (r_{ij}) \theta_{ij} \widehat{\mathbf{r}}_{ij} \tag{4}$$

where $r_{ij} = |\mathbf{r}_{ij}| = r$; $\mathbf{r}_{ij} = \mathbf{r}_i - \mathbf{r}_j$, $\widehat{\mathbf{r}}_{ij}$ is a unit vector directed along the line of centres of particles i and j, $w(r_{ij})$ is a weight function, $\mathbf{v}_{ij}$ the relative velocity between i and j, θ_{ij} is a randomly fluctuating variable with Gaussian statistics, while a_{ij}, γ and σ are constant parameters. The common choice for the conservative weight function is

$$w^C (r) = (1 - r/r_c) \tag{5}$$

which vanishes at $r = r_c$ (the cutoff distance). It is also usual to take the random force weight function to be the same as the conservative one. Fluctuation-dissipation theory [2] then provides a relationship between the magnitude of the random and

dissipative weight function magnitudes ($w^D(r) = [w^R(r)]^2$) and a relationship between σ, γ and T: $\sigma^2 = 2\gamma k_B T$.

The claimed success and popularity of DPD lies in the use of a large time step – typically an order of magnitude greater than those used in MD – a consequence of the short ranged and soft nature of the conservative force law. Groot and other workers have also extended DPD to take electrostatic interactions into account [4, 5]. DPD has been employed in a wide variety of cases including polymers [6 7], liquid crystals [8], biomolecules [9] and even cement [10]. Some rich phase behavior has been observed in DPD, giving qualitative agreement with experiment.

Despite the foregoing, DPD has a number of deficiencies. One of the more significant problems is that equations of motion lack a sound theoretical basis. Intuitively, one might expect that a course graining procedure would result in soft repulsive forces and that the microscopic fluctuations could be replaced by random and dissipative contributions. To date, no one has succeeded in deriving the force laws from statistical mechanics. In practice, either a bottom-up parametrization is obtained from Boltzmann inversion of molecular dynamics data, or, experimental values are used in a top-down parametrization [16].

Another drawback is that the equation of state generated in DPD is quadratic in the density. DPD thus cannot be used to study liquid-vapour equilibria in a single component fluid unless density dependent forces are instead used [11]. The DPD particle has been interpreted as representing N_m atoms or particles of smaller mass. This leads to scaling arguments for increased levels of coarse graining. However, Pivkin and Karniadakis [12] found an upper limit to the value of N_m, beyond which the DPD fluid freezes. Further problems arise with regard to temperature control. The basic DPD algorithm operates at constant temperature with the dissipative and stochastic forces functioning as a thermostat. However, simulations of non-equilibrium flows found that the temperature drifted at higher fields. Replacement of the DPD thermostat with the Andersen thermostat had the interesting effect that the fluid viscosity also increased [13]. Hafskjold and co-workers located the source of the temperature drift in the size of the timestep used, concluding that smaller time steps of the order of those used in molecular dynamics were necessary [14].

Groot and Warren, in their 1997 paper, state: "Indeed DPD can be viewed as a novel thermostatting method for MD". An interesting viewpoint, but one that has never been fully explored. Clearly it is desirable to have a deterministic thermostat in MD rather than a stochastic one for reasons of reproducibility, reversibility and less restriction on the magnitude of the timestep. In light of this, perhaps the word "novel" might be better replaced by "unusual" or even "poor"?

In this paper we show that the advantages of DPD – use of large time steps and an ability to show interesting phase behavior, can be obtained from molecular dynamics with a deterministic thermostat. We note here that other coarse graining strategies can be used in MD, for example methods employing MARTINI forcefields [15], for fast evaluation of phase equilibria. There is no suggestion that this DPD-like MD is superior to these methods. In section II we show how short ranged pair potentials lead to a pressure quadratic in density and an energy linear in density. Section III presents the results obtained from MD simulations using two different short ranged potentials, one based on the popular DPD weight function, and one used in Smooth Particle Hydrodynamics (SPH). It is shown that both choices give the same functional form for the pressure in single component, binary and ternary mixtures in both 2- and 3 dimensions. In section IV we generalize the result of our earlier work in which we developed a mapping between the conservative force parameters and Hildebrand solubility parameters [16], to multicomponent mixtures. In section V we present the results of using this mapping for 3D simulations using experimental data for the binary system: SnI_4 and isooctane. Finally, in section VI we summarise and draw some conclusions.

II. EQUATIONS OF STATE

The pressure, and energy (per atom) of a #-dimensional multi-component mixture are given respectively by [17]:

$$P = \rho k_B T - \frac{(\# + 1)\pi}{6}\rho^2 \sum_{i,j} x_i x_j \int_0^\infty \phi'_{ij} g_{ij}(r) r^\# dr \tag{6}$$

$$\frac{E}{N} = \frac{\# k_B T}{2} + \pi \rho(\# - 1) \sum_{i,j} x_i x_j \int_0^\infty \phi_{ij} g_{ij}(r) r^{\#-1} dr \tag{7}$$

where x_i is the number fraction (loosely referred to as mole fraction) of component i, ρ is the number density (N/V), ϕ is the pair energy function, ϕ' its first derivative while $g_{ij}(r)$ is the partial radial distribution function for particles of type i and j. Eqs. (6-7) are exact for pairwise additive potentials.

If the potential is short-ranged, vanishing at r_c, and of the form: $\phi(s; \varepsilon) = \varepsilon \phi(s)$, with $s = r/r_c$, the density dependence may be removed from the integrals in (6) and (7), giving

$$P = \rho k_B T + r_c^\# \rho^2 \sum_{i,j} x_i x_j \epsilon_{ij} \alpha_{ij} \tag{8}$$

$$E/N = \frac{\# k_B T}{2} + r_c^{(\#-1)} \rho \sum_{i,j} x_i x_j \varepsilon_{ij} \beta_{ij} \tag{9}$$

where the dimensionless quantities, α_{ij} and β_{ij}, are given by:

$$\alpha_{ij} = -\frac{(\# + 1)\pi}{6} \int_0^1 \tilde{\phi}'(s) g_{ij}(s) s^\# ds \tag{10}$$

$$\beta_{ij} = (\# - 1)\pi \int_0^1 \tilde{\phi}(s) g_{ij}(s) s^{(\#-1)} ds \qquad (11)$$

where $\tilde{\phi} = \phi/\varepsilon$. Evidently, the non-ideal part of the pressure scales $\sim\rho^2$, while the excess internal energy is linear in density. The Mayer's virial series for the pressure:

$$\begin{aligned}\frac{P}{k_B T} =& \rho + \rho^2 B_2(T) + \rho^3 B_3(T) \\ &+ \rho^4 B_4(T) + \rho^5 B_5(T) + \cdots\end{aligned} \qquad (12)$$

$$B_n = \sum_{i,j} x_i x_j B_n^{ij}(T) \qquad (13)$$

where the coefficients $B_n{}^{ij}$ are multi-dimensional integrals involving products of Mayer functions: $f_{ij} = [\exp(-\phi_{ij}/k_B T) - 1]$, would suggest the expansion could then be truncated after the 2nd term. However, Groot and Warren [3] showed that in 3 dimensions, the integral in (10) only loses its density dependence for $\rho > 3$ for a quadratic potential. Convergence of the virial expansion is expected to be poor for such high values of density, indicating that the sum of the higher order terms yields a contribution which effectively behaves as ρ^2.

The typical weight function used in DPD is a repulsive linear ramp, whose underlying pair potential is defined by:

$$\begin{aligned}\phi_{\text{DPD}} &= \frac{\epsilon_{ij}}{2}\left(1 - \left(\frac{r}{r_c}\right)\right)^2 & r < r_c \\ \phi_{\text{DPD}} &= 0 & r \geq r_c\end{aligned} \qquad (14)$$

where ϵ_{ij} is a constant with units of energy and r_c is the cutoff distance. We also consider the smooth repulsive potential:

$$\begin{aligned}\phi_{\text{SRP}} &= \epsilon_{ij}\left(1 - \left(\frac{r}{r_c}\right)^2\right)^4 & r < r_c \\ \phi_{\text{SRP}} &= 0 & r \geq r_c\end{aligned} \qquad (15)$$

This potential has found use in SPH simulations for preventing clustering of particles during relaxation of a 'mesh', but could also be used as a weight function due to its short range, being finite valued with vanishing first derivative at the origin, and the existence of three continuous derivatives which vanish at the cutoff.

III. TEST OF THE ASYMPTOTIC EQUATIONS OF STATE

In the following sections, MD simulations are conducted for one-, two- and three-component mixtures to examine whether the quantities α, β, converge to constant values independent of density.

III. 1. Single component fluids

Single component, isokinetic molecular dynamics simulations of particles governed by potentials (14) and (15) were conducted at unit temperature for a range of densities in both 2 and 3 physical dimensions. To facilitate comparison between the two different forcelaws it is necessary to scale the repulsive parameters such that the fluids have identical compressibilities. The inverse isothermal compressibility is defined by

$$\kappa_T^{-1} = \rho\left(\frac{\partial P}{\partial \rho}\right)_T \qquad (16)$$

Using eq. (16) with eq. (17) and specializing to a 1-component fluid, the scale factor is

$$\varepsilon_{\text{SR}} = \varepsilon_{\text{DPD}}\left(\frac{\alpha_{\text{DPD}}}{\alpha_{\text{SR}}}\right) \qquad (17)$$

The simulations in 2D used 1600 atoms whereas those in 3D were performed on systems of 2048 atoms. Runs were started from an initial square lattice in 2D or an fcc lattice in 3D, with 100,000 timesteps of equilibration, followed by 1,000,000 production steps (over which averages were computed). A 4th order Runge-Kutta (RK4) integrator with a timestep of 0.04 was used in all these simulations. Note that this timestep was chosen deliberately to be typical of timesteps used in DPD. A Gaussian isokinetic thermostat was used to maintain unit temperature. A range of densities were studied from 0.1 to 35 in the case of 2D simulations and 0.1 – 15 in 3D.

The first set of simulations to be described are in 3D to enable comparison with the earlier DPD work of Groot and Warren. Accordingly, we chose $\epsilon = 1$ for the DPD potential and unit cutoff. An exploratory set of simulations with the smooth repulsive force law using this same ϵ value was then conducted in order to obtain an improved value (using (17)) which was then used in subsequent runs. This gave $\epsilon = 0.46$.

Fig. 1 shows plots of the coefficients α and β for each of the two forcelaws. It is clear from the figure that beyond a density of ~3, these quantities reach a plateau, giving a value of $\alpha = 0.101$. This is in excellent agreement with Groot and Warren's DPD work. Both potentials give essentially the same value for α. β on the other hand, seems to require a higher density to reach its asymptotic value of ~0.1. The reason for this difference in behavior is presumably due to the different integrands. The integrand for β contains the pair energy function while that for α the differential of the pair energy (force).

The virial coefficients, $B_2 - B_5$, calculated for both potentials, are collected in Table 1.

B_2 was calculated using 16-point Gauss-Legendre quadrature, while higher coefficients were calculated using a hit and miss Monte Carlo scheme. Briefly, the method for estimating B_3 was as follows: a particle was placed at the origin
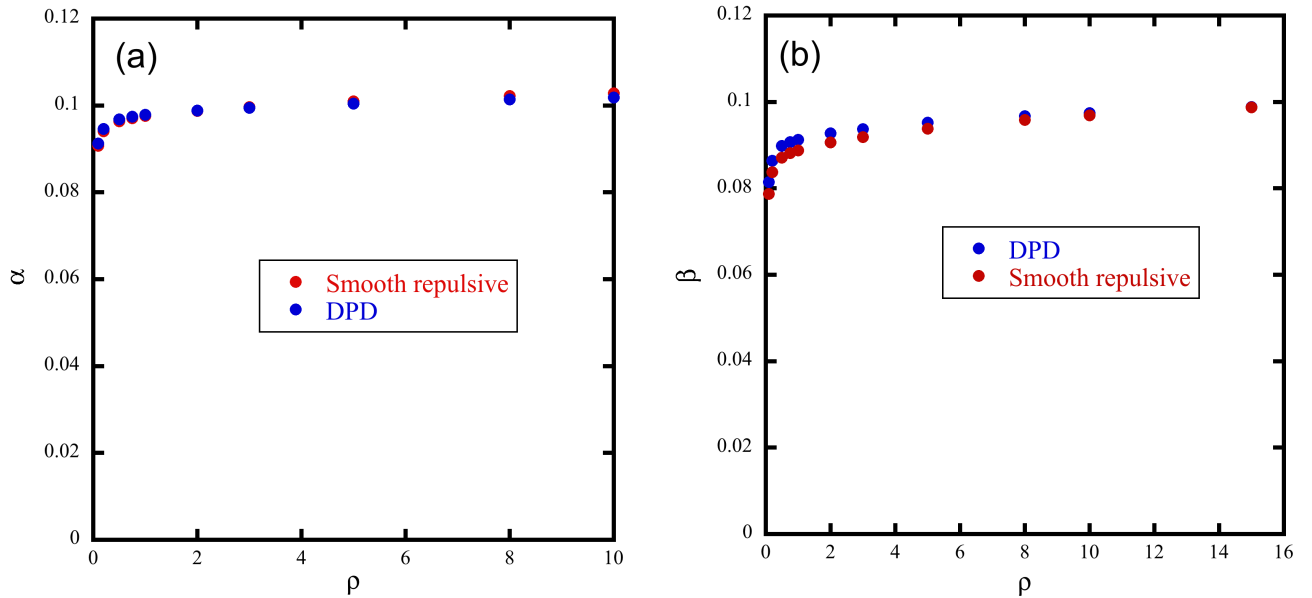
Fig. 1. Plots of the quantities α (a) and β (b) against density for the two potentials, smooth repulsive (blue circles) and DPD (red circles) in 3 spatial dimensions

and a second particle was placed randomly within a circle of radius r_c, centred on the first particle. The third particle was likewise placed randomly within a circle of radius r_c, also centred on particle 1. With the 3 particles so placed, the Mayer f-functions were calculated and then sums of the products: $f_{12}f_{13}f_{23}$ and $f_{12}f_{13}$ were compiled over 10 billion Monte Carlo trials. The third virial coefficient was then obtained from the ratio: $-4/3\{\langle f_{12}f_{13}f_{23}\rangle / \langle f_{12}f_{13}\rangle\}$. This algorithm was extended in an obvious way to compute B_4 and B_5. Full details of this algorithm, including an improvement utilising Ree-Hoover diagrams, will appear in a future publication. Fig. 2 contains plots comparing truncated virial series against the MD obtained pressure for both potentials. For either pair potential, convergence is poor – successive higher order sums overshoot the MD results, though agreement with the MD data is acceptable up to surprisingly high densities with only the quadratic B_2 term included in the sum.

For the 2D single component simulations, we chose $\epsilon = 1$ for the smooth repulsive potential and then through a similar procedure as described earlier, obtained a value of $\epsilon = 2.4$ for the DPD potential (giving the two potentials similar compressibilities). A set of simulations were conducted as per the 3D case, but spanning densities from 0.1 to 35. Fig. 3 shows plots of α and β for the two potential models. Both α and β reach asymptotic values of 0.311 and 0.30, respectively. Unlike the 2D case, in which the asymptotic values were reached at a density as low as 3, Fig. 3 shows that in 2D, the onset of the plateau requires a density ~20. Fig. 4 shows the truncated virial series for each potential compared with the MD simulation data. As with the 3D case, higher order truncations do not converge except at the lower densities. At high densities, B_2 follows the MD data more closely while the 3rd order truncation overshoots and the fourth and fifth order truncations undershoot the data.

Tab. 1. Virial Coefficients at $T = 1$ for a single component fluid modelled using the two forcelaws defined by (14) and (15) in both 2 and 3 dimensions

		ϵ	B_2	B_3	B_4	B_5
2D	$\frac{\epsilon_{ij}}{2}\left(1-\left(\frac{r}{r_c}\right)\right)^2$	2.4	0.25233	0.019527	-0.0031404	-0.0001201
3D		1.00	0.09773	0.0009079	-0.0001006	9.673e-06
2D	$\epsilon_{ij}\left(1-\left(\frac{r}{r_c}\right)^2\right)^4$	1.00	0.24373	0.020857	-0.0025799	-0.0003161
3D		0.46	0.09716	0.001205	-0.0001198	9.2887e-06
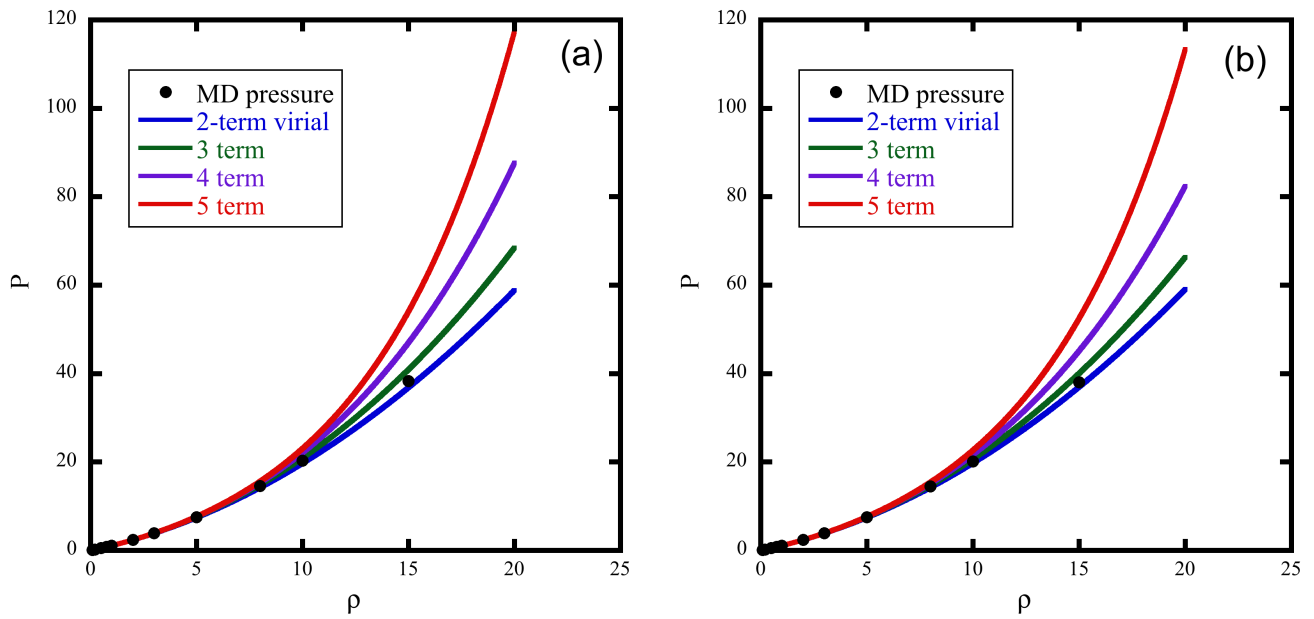
Fig. 2. Unit temperature isotherms (circles) and partial sums of the virial expansion (lines) for the smooth repulsive potential (a) and the DPD potential (b) in 3 spatial dimensions
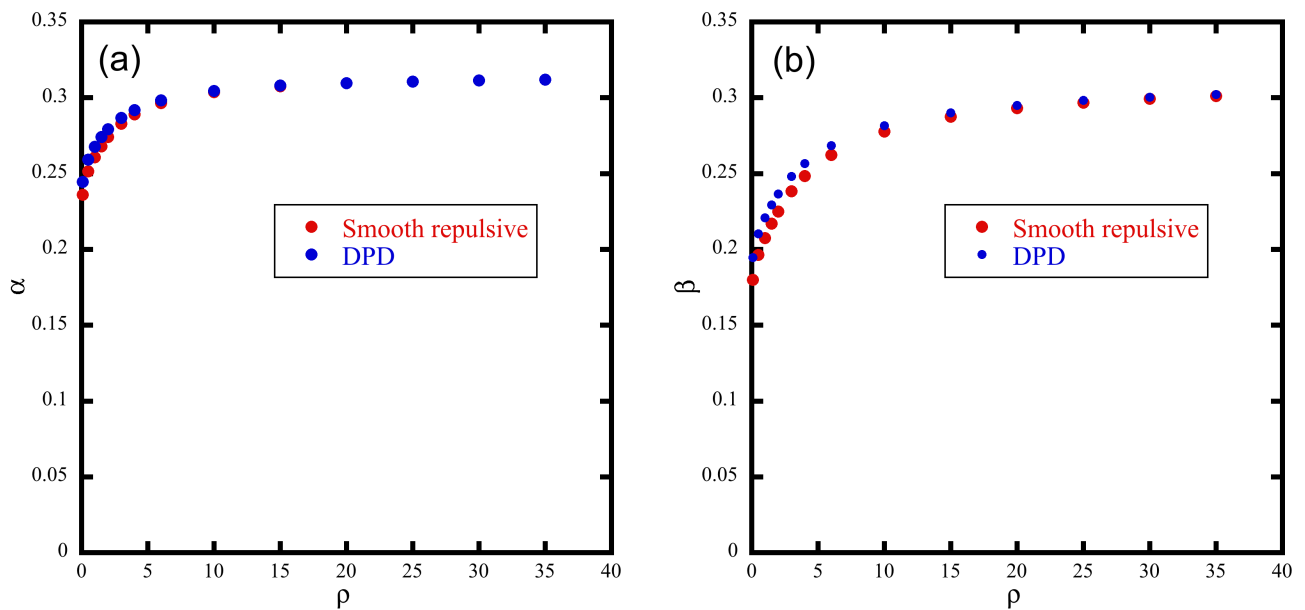
Fig. 3. Plots of the quantities α (a) and β (b) against density for the two potentials, smooth repulsive (blue circles) and DPD (red circles) in 2 spatial dimensions
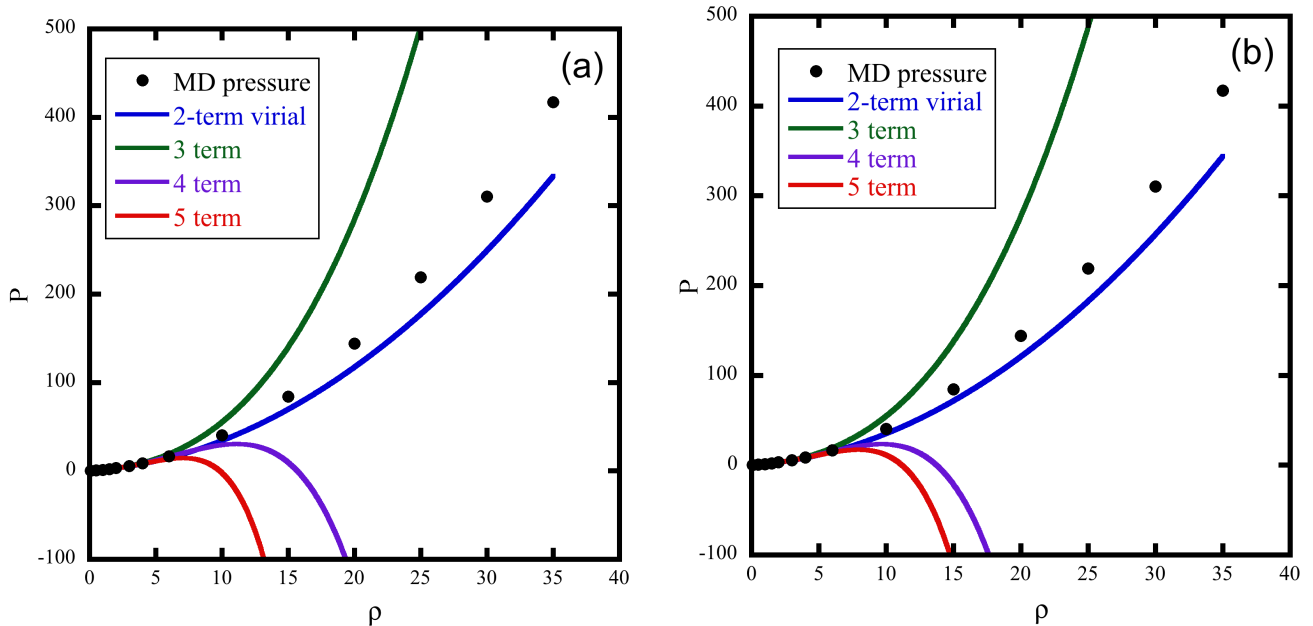
Fig. 4. Unit temperature isotherms (circles) and partial sums of the virial expansion (lines) for the smooth repulsive potential (a) and the DPD potential (b) in 2 spatial dimensions

III. 2. Binary fluid mixtures

For binary and higher order mixtures, it is of interest to know if the value of α also reaches an asymptotic value and if so, is there any composition dependence. Furthermore, we wish to test the assumption of both Travis *et. al.* [16] and Maiti and McGrother [18] that the component α_{ij}'s have the same value as a composition weighted α in mixtures. To answer these questions, binary mixtures were conducted in 2 physical dimensions (for computational efficiency) for the smooth repulsive potential at two different compositions: an equimolar (1:1) mixture and a 1:3 composition of the two types of particle (which we henceforth refer to as Xenon and Krypton). For convenience we chose $\varepsilon_{11} = 1$, $\varepsilon_{22} = 1$ and $\varepsilon_{12} = 1.5$ to encourage segregation. A range of densities were explored between 0.1 and 35 with 1600 particles in total. The temperature was maintained at unity using a Gaussian isokinetic thermostat.

Fig. 5 shows a plot of the α_{ij}'s as a function of density for the two compositions. These figures show that all of the α's reach a plateau at the same density ~20 as for the single component 2D example. The curve for α_{11} in Fig 5b does not appear to converge as well as the others. This is likely a consequence of the smaller number of type 1 particles in the simulation box – giving rise to larger errors. It may also be an indication that the timestep of 0.04 is a little too large at the higher densities. In the equimolar case, $\alpha_{11} = \alpha_{22} \neq \alpha_{12}$. However, a mean α, defined by the weighted

sum: $\langle \alpha \rangle = \sum_i \sum_j \varepsilon_{ij} \alpha_{ij} x_i x_j$, is also constant and close in magnitude to the single component α for this potential (0.323 *cf* 0.311). In the case of the 1:3 mixture, $\alpha_{11} \neq \alpha_{22} \neq \alpha_{12}$. Despite this, the weighted α is again similar in value to the single component case (0.323), suggesting there is no composition dependence on the average α. However, there are implications for the mapping with regular solution theory (see later section).

Fig. 6 shows typical snapshots from the simulations at a density of 20. Both images show almost complete separation. The interface is close to linear for the equimolar mixture while the 1:3 mixture forms a roughly circular droplet (when the periodic boundary conditions are taken into account). If we now examine snapshots from a density at which the component α_{ij}'s have not yet reached their plateau value, say $\rho = 10$, then it is evident that segregation is incomplete for both compositions (Fig. 7).

Virial coefficients for the two mixtures were calculated using the composition weighted sum of the B_n^{ij}. One additional set of data (to that in Table 1) needed is that for $\epsilon_{12} = 1.5$. These coefficients, $B_2 - B_5$, were determined to be: {0.32726, 0.0481326, −0.00321385, −0.00206103}. Truncated virials series are compared against the raw simulation data in Fig. 8. As expected, the density dependence is similar to that seen in the 1 component case, namely that the B_2 series follows the data closest over the entire range. Higher order truncations fit the data more accurately at lower densities, but then diverge at higher densities.
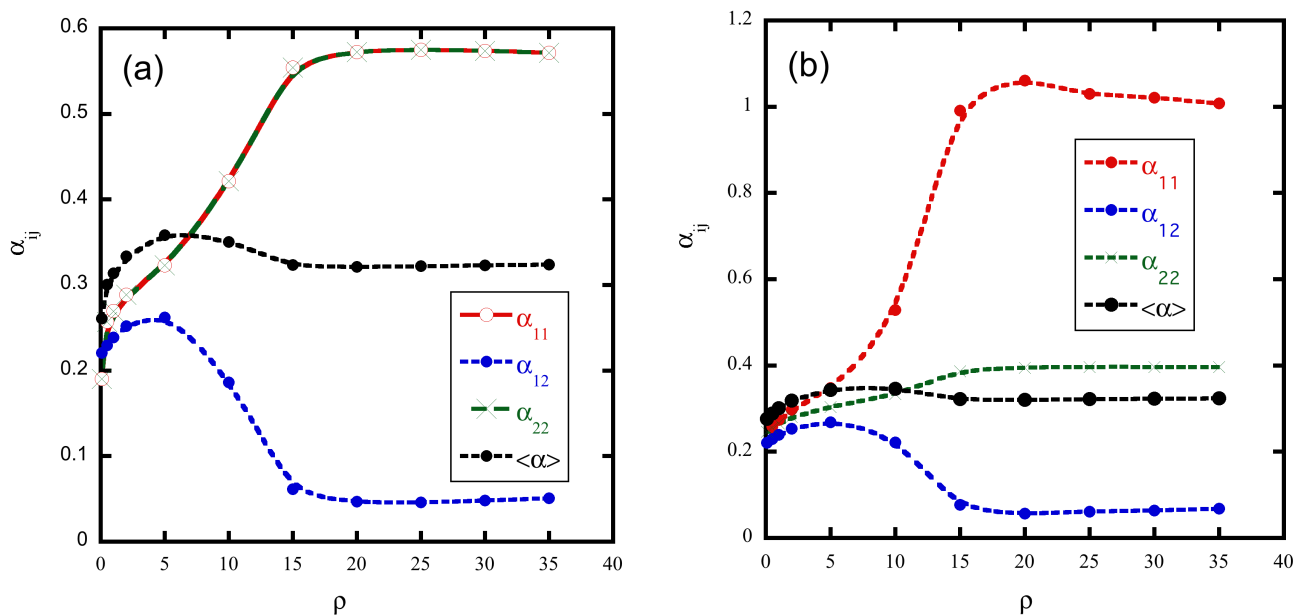
Fig. 5. Plots of the various α's against density for Xe/Kr mixtures at unit temperature (a) 1:1 mixture, (b) 1:3 mixture
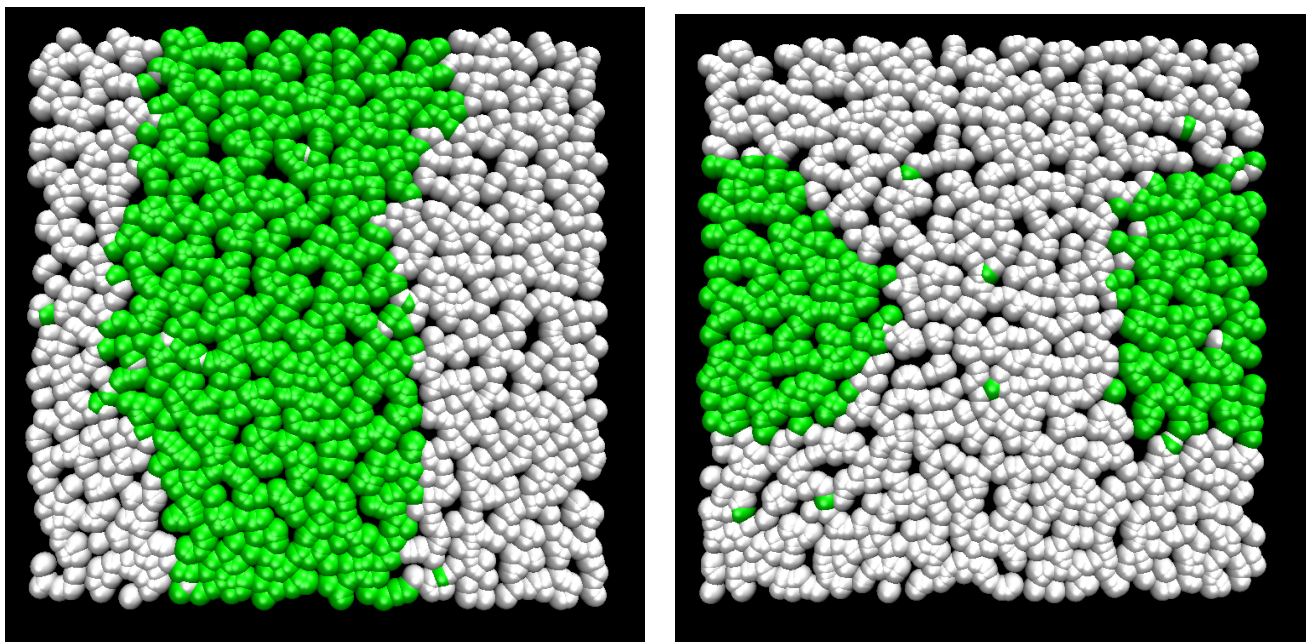
Fig. 6. Snapshots (after 1 million steps) from simulation of 1600 soft repulsive disks with $\varepsilon_{11} = \varepsilon_{22} = 1$; $\varepsilon_{12} = 1.5$, $\rho = 20$, $T = 1$. Left image is 1:1 mixture, right image is 1:3 mixture
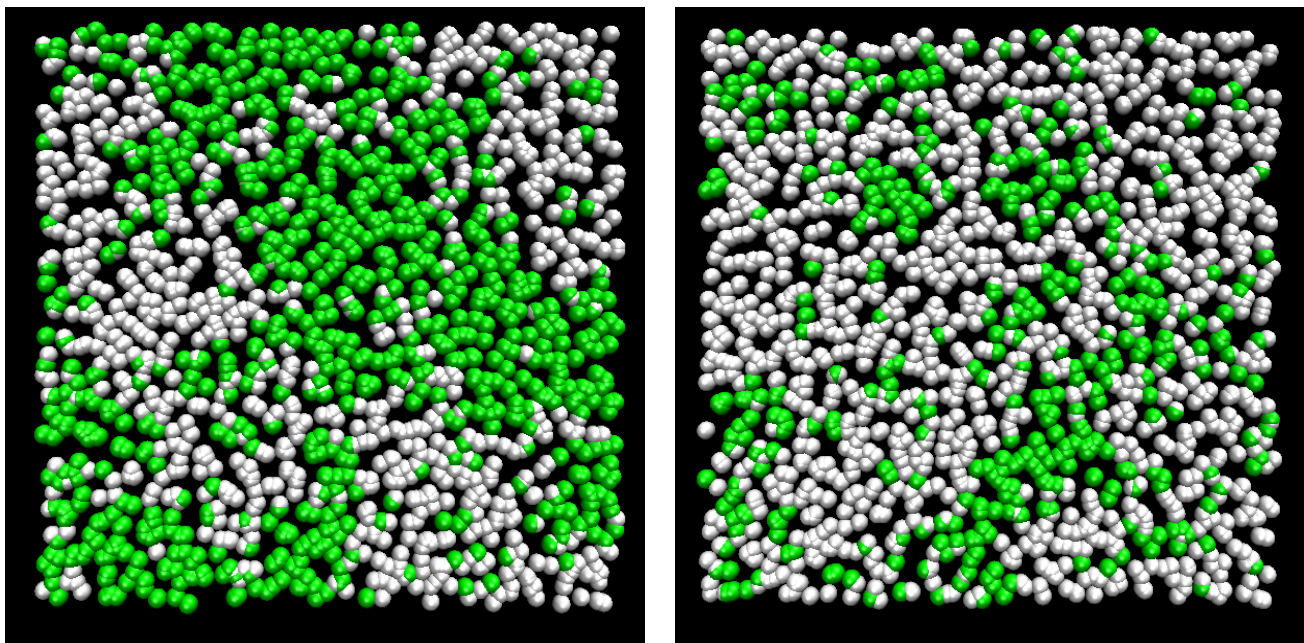
Fig. 7. Snapshots (after 1 million steps) from simulation of 1600 soft repulsive disks with $\varepsilon_{11} = \varepsilon_{22} = 1$; $\varepsilon_{12} = 1.5$, $\rho = 10$, $T = 1$. Left image is 1:1 mixture, right image is 1:3 mixture
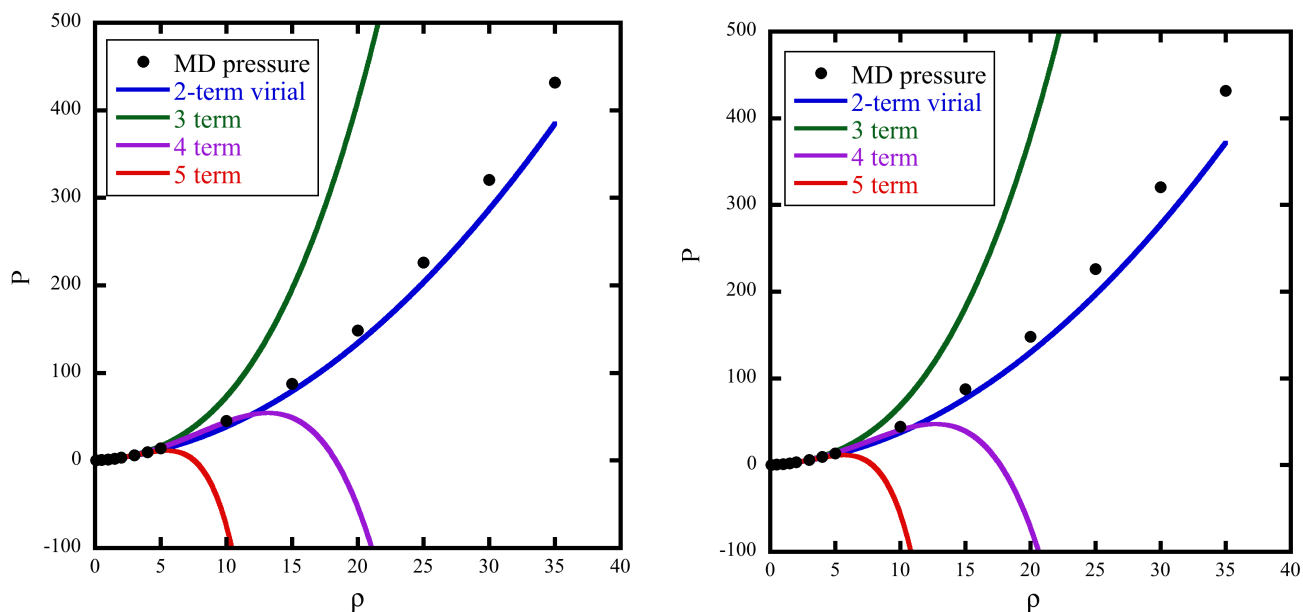
Fig. 8. Unit temperature isotherm (circles) and partial sums of the virial expansion (lines) for the smooth repulsive potential in 2 spatial dimensions. Left picture is 1:1 mixture, right picture is 1:3 mixture

III. 3. Ternary fluid mixtures

To demonstrate that the findings described in the previous sections are not restricted to binary mixtures, simulations of an equimolar 2D ternary mixture ($x_1 = x_2 = x_3 = 1/3$) were conducted at unit temperature and at densities of $\rho = 20, 30, 35, 40$ and 45 for the smooth repulsive potential. These systems contained 2400 atoms (800 of each species type). The repulsive parameters were chosen somewhat arbitrarily to encourage segregation: $\epsilon_{11} = \epsilon_{22} = \epsilon_{33} = 1.0$; $\epsilon_{12} = 1.25$, $\epsilon_{13} = 1.5$, $\epsilon_{23} = 1.35$. Each of these simulations were run from initial square lattice configurations for 100,000 timesteps followed by production runs of 1 million steps.

The density dependence of the α's is displayed in Fig. 9 (values in Table 2). The mean α, defined as $\langle \alpha \rangle = \sum_i \sum_j \varepsilon_{ij} \alpha_{ij} x_i x_j$, is fairly constant, having a value of 0.325 (which is close to the values obtained for single component and binary mixtures). The component α's also attain plateau values, but for densities > 30 (compare for the binary mixture case).
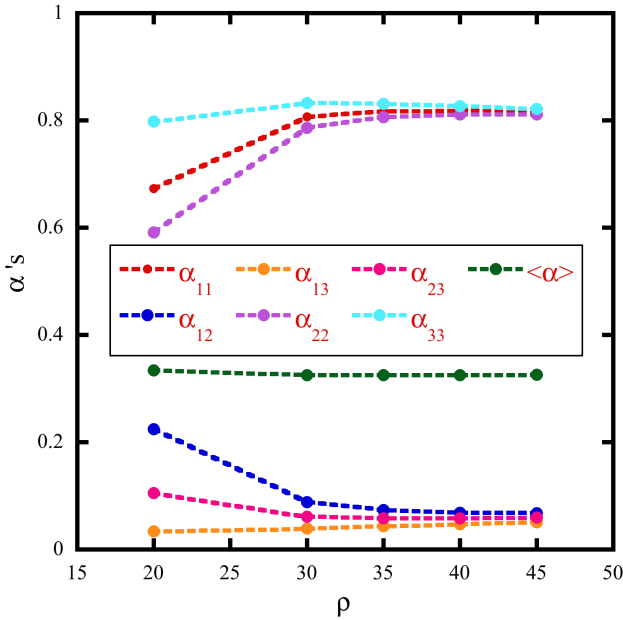
Fig. 9. Density dependence of α_{ij}'s and $<\alpha>$ for a 2D equimolar ternary mixture of soft repulsive disks at $T = 1$

Snapshots taken from the end of the production run simulations (1 million steps) at a density in the plateau region for the α_{ij}'s ($\rho = 45$) and from just before this regime ($\rho = 20$) are shown in Fig. 10. It is again evident that full segregation is associated with constancy of the α_{ij}'s.

IV. MAPPING WITH REGULAR SOLUTION THEORY (RST)

In their 2007 paper, Travis *et al.* showed that the Groot-Warren formulation of DPD for binary mixtures was iso-

morphic to regular solution theory (RST). The isomorphism should also apply to MD provided the potentials are soft, short ranged and repulsive leading to constant asymptotic α's. The results presented in Section III strongly suggest this will indeed be the case. In this section, we summarise the main elements of the mapping, but generalise it to handle multicomponent mixtures.

An equation of state which is volume-explicit can be integrated to yield the Helmoltz free energy of the mixture [19]:

$$
A_{mix} = \int_V^\infty \left(P - \frac{n_T RT}{V} \right) dV \\
- RT \sum_i n_i \ln \left(V/n_i RT \right) + \sum_i n_i \left(u_i^0 - T s_i^0 \right)
\tag{18}
$$

where R is the universal gas constant, n_T is the total amount of substance, V is the extensive total volume, n_i the amount of substance of component i, while $u^0{}_i$ and $s^0{}_i$ are, respectively, the molar internal energy and molar entropy of an ideal gas of pure component i. The equation of state (8) yields the following free energy (in 3D):

$$
\frac{A_{mix}}{n_T} = \frac{r_c^3 n_T N_A^2}{V} \sum_i \sum_j x_i x_j \epsilon_{ij} \alpha_{ij} \\
- RT \sum_i x_i \ln \left(\frac{V}{n_i RT} \right) + \sum_i n_i \left(u_i^0 - T s_i^0 \right),
\tag{19}
$$

where N_A is Avogadro's constant.

The free energy of mixing, A^M, is defined as the free energy of the mixture relative to the mole fraction weighted sum of the pure component free energies:

$$
\frac{A^M}{n_T} = \frac{A_{mix}}{n_T} - \sum_i x_i \left(\frac{A_i}{n_i} \right)
\tag{20}
$$

The excess free energy of mixing is

$$
\frac{A^{M,E}}{n_T} = -\frac{r_c^3 N_A^2 \nu}{2} \left[\sum_i \sum_j B_{ij} \varphi_i \varphi_j \right],
\tag{21}
$$

where v is the molar volume of the mixture, φ_i is the volume fraction of component i and B_{ij} is defined by

$$
B_{ij} = \frac{\varepsilon_{ii} \alpha_{ii}}{v_i^2} + \frac{\varepsilon_{jj} \alpha_{jj}}{v_j^2} - 2 \frac{\varepsilon_{ij} \alpha_{ij}}{v_i v_j},
\tag{22}
$$

in which v_i is the molar volume of pure component i (there is no volume change on mixing in RST, hence molar volumes of the pure components and partial molar volumes are identical). The entropy of mixing is given by

$$
\frac{S^M}{R} = -\sum_i x_i \ln \varphi_i
\tag{23}
$$

Tab. 2. Values of $\{\alpha_{ij}\}$ and $<\alpha>$ for equimolar ternary mixture of soft repulsive disks at $T = 1$

		α_{11}	α_{12}	α_{13}	α_{22}	α_{23}	α_{33}	$<\alpha>$
	20	0.6732	0.2240	0.03372	0.5916	0.10502	0.7980	0.3342
	30	0.8066	0.0880	0.03913	0.7862	0.06104	0.8326	0.3253
ρ	35	0.8169	0.0738	0.0436	0.8056	0.0579	0.8308	0.3250
	40	0.8185	0.0688	0.0473	0.8113	0.0581	0.8265	0.3252
	45	0.8162	0.0676	0.0506	0.8115	0.0594	0.8213	0.3256

Hildebrand gives the following expression for the molar heat of mixing [20]

$$\Delta H_{mix} = \frac{v}{2} \sum_i \sum_j (\delta_i - \delta_j)^2 \varphi_i \varphi_j \qquad (24)$$

where the δ's are solubility parameters and the geometric mixing rule has been assumed.

Evidently, dynamics with short ranged repulsive potentials is closely isomorphic to regular solution theory. Phase separation is therefore expected depending on the form of the free energy surface. The mapping between the solubility parameters and the repulsive parameters, ε_{ij} is given by

$$(\delta_i - \delta_j)^2 = -r_c^3 \left(\rho_i^2 \varepsilon_{ii} \alpha_{ii} + \rho_j^2 \varepsilon_{jj} \alpha_{jj} - 2\rho_i \rho_j \varepsilon_{ij} \alpha_{ij} \right) \qquad (25)$$

Both Groot and Warren [3] and Travis and co-workers [16] assumed (without proof) that all the α_{ij} were equal. If (25) is taken as a definition, knowledge of the left hand side for a particular pair of components enables the appropriate portion of the repulsive parameter matrix to be determined. The procedure outlined in Ref 16 entails first calculating the like-like terms from the following relationship:

$$\varepsilon_{ii} = \frac{\delta_i^2}{\alpha_{ii} \rho_i^2 r_c^3} \qquad (26)$$

following which the cross terms may then be obtained from Eq. (25).

V. COMPARISON BETWEEN MD AND RST

In this section we demonstrate how to utilize the mapping between molecular dynamics with short range repulsive potentials and regular solution theory. Experimental data on solubility differences measured for a binary mixture of C_8H_{18} and SnI_4 were used to obtain the repulsive parameters $\{\epsilon_{ij}\}$ from Eqs. (25-26). This system was chosen both for its close conformity to RST and the existence of solubility parameters value at 2 different temperatures.

The first step of the comparison entails using RST to generate a binodal curve. Within this theory, the free energy of mixing (for a 2 component system) as a function of composition is given by

$$\begin{aligned} A^M = & RT \left(x_1 \ln x_1 + x_2 \ln x_2 \right) \\ & + (v_1 x_1 + v_2 x_2)(\delta_1 - \delta_2)^2 \varphi_1 \varphi_2 \end{aligned} \qquad (27)$$

In what follows we take SnI_4 as component 1. Once the molar volumes and solubility parameters are known as a function of temperature, a set of free energy curves may be plotted against composition, each at a different temperature. The binodal curve is then constructed from the set of coexisting mole fractions obtained using a double tangent construction.
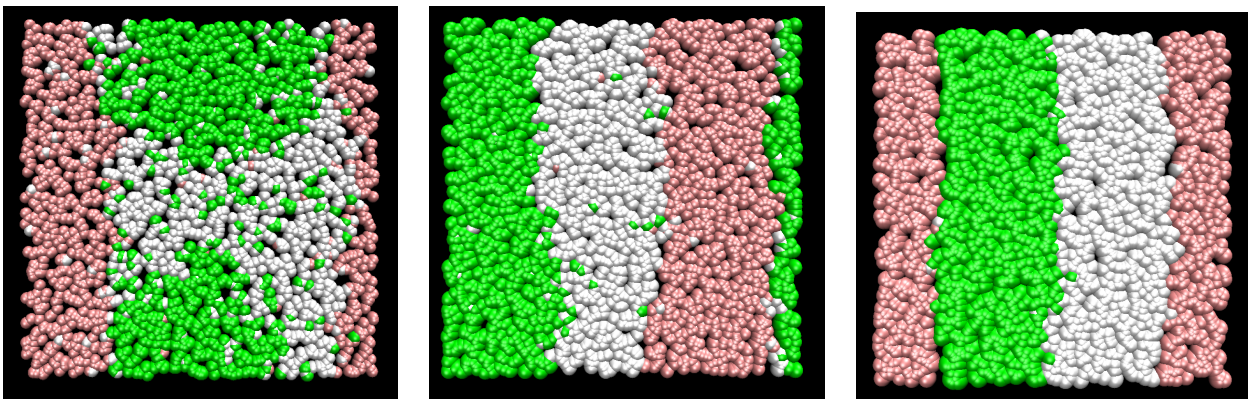
Fig. 10. Snapshots (after 1 million steps) from 2D equimolar ternary mixture of soft repulsive disks at $T = 1$ for different densities: $\rho = 20$ (left), $\rho = 30$ (center) and $\rho = 45$ (right)

For isooctane, Hildebrand and Scott [20] list values for molar volume, and solubility parameter at the two temperatures: 298 K and 372 K (see Table 3). The same textbook provides the following useful relationship:

$$\frac{d\,(\ln \delta)}{d\,(\ln V)} = -\frac{n+1}{2} \tag{28}$$

where n is an empirical parameter. For isooctane, the calculated value of n was determined to be 1.2528. Eq. (28) was then used to estimate isooctane solubility parameters at all other temperatures.

For SnI_4, we fitted the molar volume-temperature data contained in the paper by Hildebrand and Negishi [21] to the following equation: $V(T)/cm^3 = 116.03 + 0.11796*(T/K)$. The solubility parameters were generated from the equation: $\ln[\delta/(cal^{1/2} cm^{-3/2})] = 2.9106 - 0.0016474 \,(T/K)$ which was obtained from a least squares fit to the data given in the paper by Travis *et. al.* [16].
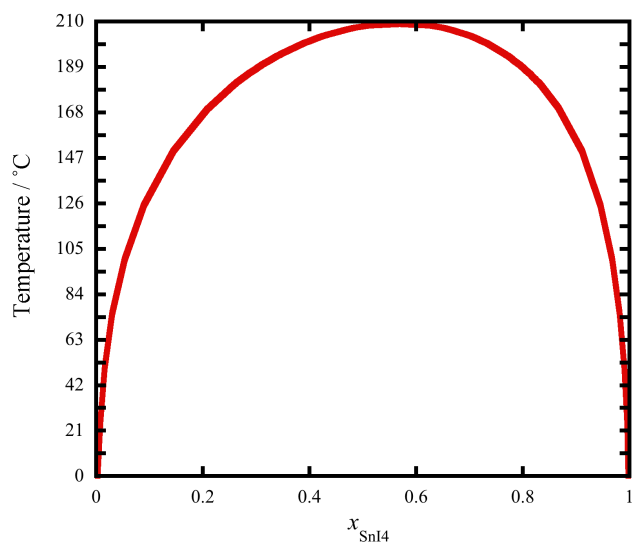
Fig. 11. Binodal curve for the system: SnI_4/C_8H_{18}, as calculated using Regular Solution Theory

Free energy curves were then generated over a temperature range of 0°C – 220 °C, the upper end being well above the known upper critical solution temperature. The double tangent problem was solved using a Newton-Raphson method

iterative scheme and the resulting binodal curve is shown in Fig. 11.

Molecular dynamics simulations were conducted of binary mixtures (in 3D) using the DPD potential. To obtain the repulsive parameters for use in these simulations, the following steps were taken. First, simulations of equimolar mixtures of repulsive spheres were conducted at unit temperature and a range of densities from $\rho = 0.1$ to $\rho = 6$. In these simulations the matrix of repulsive parameters was taken (arbitrarily) to be $\epsilon_{11} = 1.0$, $\epsilon_{22} = 1.2$, $\epsilon_{12} = 1.5$. The behavior of the component α's and the mean α with density are shown in Fig. 12. From Fig. 12 it is apparent that beyond a density of around 3, the component α's reach plateau values of $\alpha_{11} = 0.101$, $\alpha_{22} = 0.101$, $\alpha_{12} = 0.098$, $<\alpha> = 0.130$.
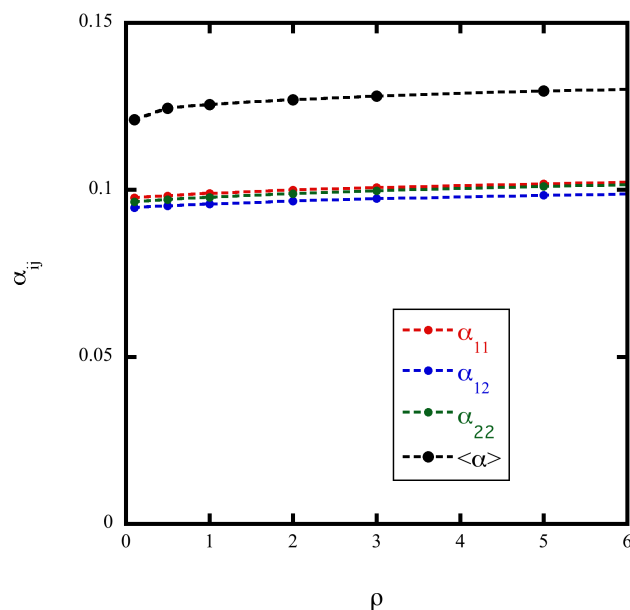
Fig. 12. Component α's and mean α for 3D binary equimolar solutions of DPD spheres as a function of density

These asymptotic α's were then used to derive repulsive parameters within the framework of the mapping between MD and RST. In DPD, the usual choice of dimensionless quantities uses r_c as a convenient length scale, k_BT as a convenient energy scale and the mass of a molecule as the basic unit of mass.

Tab. 3. Thermodynamic data for pure SnI_4 and isooctane. The use of non-SI units is to facilitate comparison with earlier published work on RST

	T / K	V/ (cm^3 mol^{-1})	δ/(cal$^{1/2}$ cm$^{-3/2}$)
isooctane	298	166	6.85
	372	184	6.1
SnI_4	298	151.1	11.7
	637.5	191.23	6.43

Tab. 4. Densities and repulsive parameters (all in reduced units) for 3D binary mixtures used in the SnI_4/isooctane simulations. Component 1 is SnI_4, while 2 is isooctane

T/ °C	$\overline{\rho}$	ϵ_{11}	ϵ_{22}	ϵ_{12} ($= \epsilon_{21}$)
0	5.4717	65.1425	28.1379	55.2691
100	4.9159	39.4747	19.7052	35.9919

Thus $\overline{\rho} = \rho r_c^3$, $\overline{\varepsilon} = \frac{\varepsilon}{k_B T}$, $\overline{\delta} = \delta \sqrt{\left(\frac{r_c^3}{k_B T}\right)}$, *etc.* Taking $\overline{\rho}$ = 4 (safely in the regime where the α's attain their asymptotic value), and using the highest molar volume of the mixture of SnI_4/isooctane across the range of temperatures studied (v_{mix} = 211 cm^3 mol^{-1}) gave an r_c = 11.191 Å. Dimensionless component densities and solubility parameters were then calculated using this value of r_c and the appropriate value of k_BT for each temperature of interest. Non-dimensionalised versions of Eqs. (25-26) were then used to obtain the reduced unit values of the repulsive parameters (see Table 4).

Isokinetic MD simulations were conducted of equimolar mixtures of DPD spheres at two different temperatures (0°C, 100°C). Each simulation was conducted in reduced units and therefore the temperature in each case was maintained at the value of unity by a Gaussian thermostat. The system density in each case is given in Table 4. These simulations, employing 42592 atoms with initial configurations based on fcc lattices, were run for 50,000 steps, followed by 50,000 production steps. The equations of motion were integrated using a 4th

order Runge Kutta integrator using a reduced timestep of 0.04.

Snapshots – taken at the end of 50,000 production steps for both temperatures – are displayed in Fig. 13.

From the figure it is evident that the system has split into 2 phases with roughly planar interfaces separating them. At 0°C, the phase rich in isooctane (middle slab) has a regular (crystalline) arrangement of particles, which is absent at 100°C. This may seem counterintuitive given *pure* bulk isooctane has a larger molar volume than SnI_4. However, the simulations are conducted at constant volume, and the SnI_4 particles repel each other more strongly than do isooctane particles (see ϵ values in Table 4). In a mixture of the two components, the SnI_4 pack less efficiently than isooctane particles. Since the DPD potential bears no relation to the true pair potential for these molecules, no physical significance can be attached to the spatial arrangement of particles. The solid-like nature of the isooctane-rich phase is therefore an artefact of the method (this will also be the case in DPD).
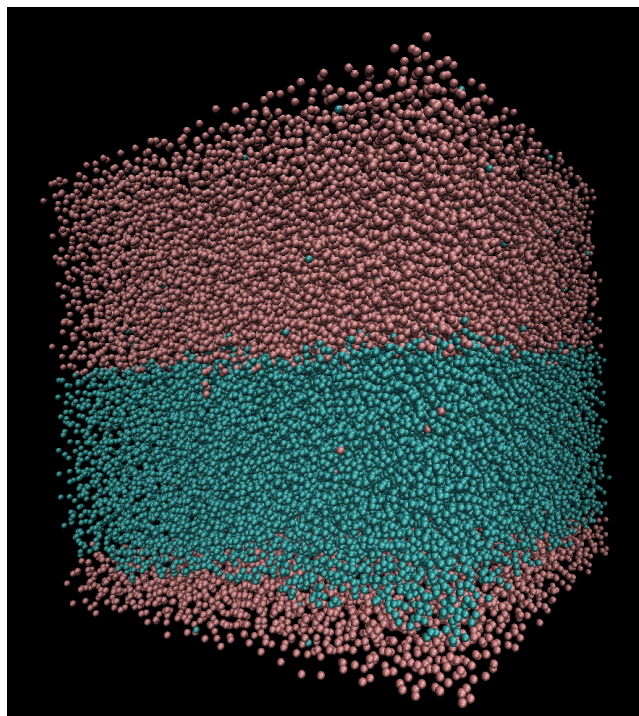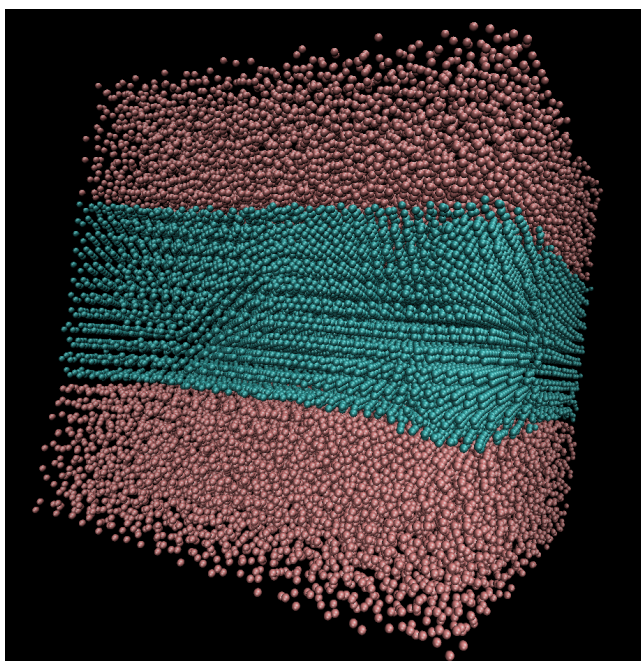
Fig. 13. Snapshots from the 3D binary equimolar mixtures of SnI_4 (red colored particles) and isooctane (green colored particles) at two different temperatures: 0°C (left), 100°C (right)

Visual inspection of the configurations reveals an increased impurity of the two phases at the higher temperature. To quantify the phase composition, we have used the method introduced by Gelb and Müller [22]. Briefly, this entails calculating coarse grained measures of density and composition, which are then adjusted to remove particles deemed to lie in an interface. The density and composition of any co-existing phases is then easily obtained once the subcells have been sorted based on whether their density or composition lies within a specific range characteristic of these phases. The process (carried out post-run) entails a number of stages. In the first stage, a cutoff radius is chosen and then based on this, all atoms in the system are visited in turn to produce a list of their neighbours and species type falling within a sphere defined by this radius, and centered on that atom.
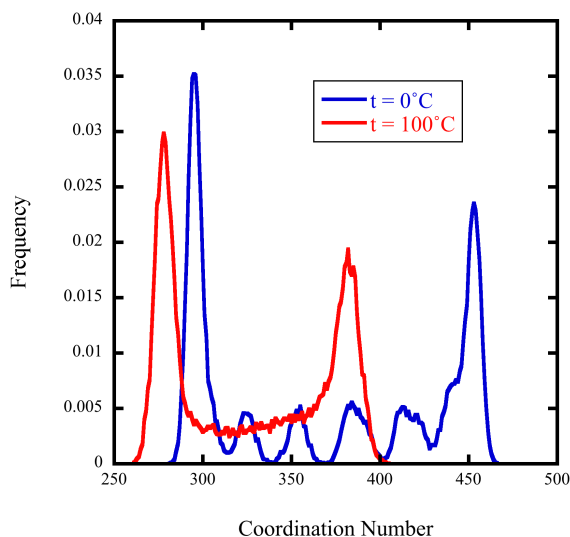
Fig. 14. Coordination numbers for equimolar mixtures of isooctane/SnI$_4$ at t = 0°C (blue line) and t = 100°C (red line)

Histograms of these coordination numbers then reveal the existence of 2 or more phases. Several trial cutoff radii are explored and a compromise is then made resulting in good separation of the peaks in the histogram and gaining good statistics. In the second stage, the simulation cell is divided into cubes (subcells) within which the density and composition is calculated. Any subcell in which more than 30% of its occupants have a number of neighbours between the values

of the peaks in the coordination number histogram is then deemed to be part of the interface between those phases. An interfacial subcell (and its occupants) is then removed from the next stage of the analysis which entails calculating histograms of density and composition from which the density and composition of these phases can then be determined.
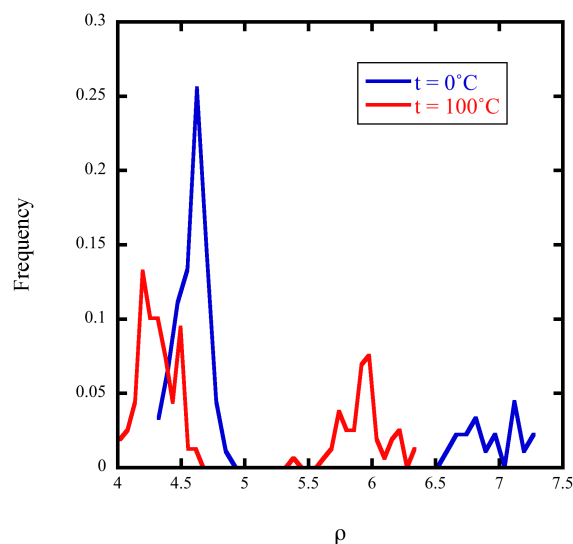
Fig. 15. Density distributions for equimolar mixtures of isooctane/SnI$_4$ at $t = 0°C$ (blue line) and $t = 100°C$ (red line). Note that these distributions were obtained using the 'clean-up' procedure outlined by Gelb and Müller

In this work we found that a cutoff of 2.5 gave clear results for the coordination number histograms, while a $7 \times 7 \times 7$ division of the simulation cell resulted in useable density/composition histograms at 0°C whereas $6 \times 6 \times 6$ was optimum at 100°C. Rather than using the number of neighbours of an atom, we used the number of neighbours of a given *type* (SnI$_4$ in the present case), when deciding which subcells to eliminate from the analysis. Division into the 2 phases was then based on the mole fraction of SnI$_4$ in any subcell compared with the range of values from the composition histogram. The process is illustrated in Figs. 14-15 which respectively show coordination number histograms, and density histograms at 0°C and 100°C.

Tab. 5. Composition and density of each phase for binary equimolar mixture of SnI$_4$ and isooctane. Data obtained using the Gelb and Müller procedure

	0°C		100°C	
	x_{SnI4}	ρ	x_{SnI4}	ρ
Phase 1	0.000	6.93	0.003	5.89
Phase 2	1.000	4.54	0.992	4.27
Interface	0.452	5.57	0.524	4.836

Both histograms (density and coordination number) are bimodal, with the main peaks coming closer together as temperature increases (they would be expected to coalesce near the upper critical solution temperature). The minor peaks in the 0°C data of Fig. 14 indicate layering in the interfacial region adjacent to the crystalline phase. The two phases have markedly different densities. By counting the number of each type of particle within the subcells, values of the composition in each of the main phases can be obtained. Table 5 gives the data obtained for this system. During the analysis it was apparent that a high percentage of the subcells constituted the interface, possibly indicating the run lengths were too short. The use of an elongated simulation box can be expected to reduce the volume fraction of the interface. The values for the mole fraction of SnI_4 in each of the two phases confirms what was seen in the snapshots, namely that there is a small increase in SnI_4 in phase 1 at the higher temperature. The binodal curve in Fig. 11 has very steep boundaries with two almost pure phases predicted: SnI_4 mole fractions of 0.0033 and 0.998 at 0°C; 0.054 and 0.968 at 100°C, in line with our MD results of the same system. Clearly more data using larger system sizes and longer simulation times are required for a full systematic and quantitative comparison with RST. Such a study is currently underway and the results will be published at a later date. However, the results contained in this section suggest that the mapping between a DPD-like MD and RST holds true and the methodology for applying this to other systems, including those with more than 2 components is straightforward, if a little tedious.

VI. SUMMARY AND CONCLUSIONS

It has been demonstrated that the main features of DPD may be obtained using molecular dynamics employing a deterministic thermostat. This isomorphism holds as long as the MD pair potentials are sufficiently smooth and short ranged, which gives rise to a quadratic equation of state (pressure as a function of density). Indeed, it has been argued that DPD could be considered as MD with an unorthodox thermostat. Using MD in place of DPD removes the problematic stochastic forces which require specially formulated integration schemes. Additionally, it would allow non-equilibrium simulations to be run under isothermal conditions without the need for additional thermostatting as is frequently required in DPD to counteract the notorious temperature drift.

Simulations carried out in 2 and 3 physical dimensions as well as for single, binary and ternary mixtures confirm that a quadratic equation of state is always obtained. Two different pair potentials were compared and found to give comparable results. In practice, the choice of potential will be a compromise between smoothness and the minimum density that needs to be used in order to guarantee the quadratic equation of state. For instance, a pair potential based on the DPD conservative force weight function requires a density greater than 3 in reduced units whereas the smooth repulsive potential (Eq. 15) requires a density of 10 which will give rise to a greater number of pair interactions to calculate. This minimum density increases when we change from 3 dimensions to 2 dimensions or the number of components increases from two to three.

We have extended the mapping between regular solution theory and DPD (and therefore MD-like DPD) first introduced by Travis *et al* [16]. for binary mixtures to multicomponent mixtures. The equation for obtaining the repulsive parameters is formally the same for > 2 components with the proviso that it is used on each *binary pair* of species. The mapping and methodology have been demonstrated for a equimolar binary mixture known to conform to RST, namely SnI_4 and isooctane. MD simulations were conducted at two different temperatures giving results broadly in line with the predictions of the theory, with two almost pure phases present at both temperatures. The correspondence between DPD and RST results from each having the same mathematical form for the Helmoltz energy of mixing. It seems unlikely that DPD (or DPD-like MD) can yield any deeper physical significance about phase equilibria though more research is required to explore this point further.

There is no reason why MD cannot be used in all the applications which have been so far been explored using DPD. The advantage of having a far simpler algorithm without the problems connected with stochastic forces is to be welcomed. The maximum timestep which could be used in MD simulations of purely repulsive, structureless particles is controlled by the type of potential function and the integration algorithm employed. Softer potentials allow for a larger timestep while smoothness, especially at the truncation point will provide more accurate trajectories. In this work the RK4 integration scheme was employed to improve accuracy at larger timesteps. The timestep used in the present work (0.04) was selected for comparison with earlier DPD publications and is on the cusp of what is acceptable for the potentials and densities employed. The DPD potential gave better energy conservation than the smooth repulsive potential with this timestep size.

Bibliography

[1] P.J. Hoogerbrugge, J.M.V.A. Koelman, *Simulating microscopic hydrodynamic phenomena with dissipative particle dynamics*, Europhys. Lett. **19**, 155 (1992).

[2] P. Español, P.B. Warren, *Statistical Mechanics of Dissipative Particle Dynamics*, Europhys. Lett. **30**, 191 (1995).

[3] R.D. Groot, P.B. Warren, *Dissipative Particle Dynamics: Bridging the gap between atomistic and mesoscopic simulation*, J. Chem. Phys. **107**, 4423 (1997).

[4] R.D. Groot, *Electrostatic interactions in dissipative particle dynamics – simulation of polyelectrolytes and anionic surfactants*, J. Chem. Phys. **118**, 11265 (2003).

[5] M. González-Melchor, *Electrostatic interactions in dissipative particle dynamics using the Ewald sums*, E. Mayoral,

M.E. Velázquez, J. Alejandre, J. Chem. Phys. **125**, 224107 (2006).

[6] R.D. Groot, *Mesoscopic Simulation of Polymer-Surfactant Aggregation*, Langmuir **16**, 7493 (2000).

[7] F. Goujon, P. Malfreyt, D.J. Tildesley, *Mesoscopic simulation of entanglements using dissipative particle dynamics: application to polymer brushes*, J. Chem. Phys. **129**, 034902 (2008).

[8] S. Jury, P. Bladon, M. Cates, S. Krishna, M. Hagen, N. Ruddock, P. Warren, *Simulation of amphiphilic mesophases using dissipative particle dynamics*, PCCP **1**, 2051 (1999).

[9] J. Shillcock, R. Lipowsky, *Visualizing soft matter: mesoscopic simulations of membranes, vesicles and nanoparticles*, BioPhys. Rev. and Lett. **2**, 33 (2007).

[10] N.S. Martys, *Study of dissipative particle dynamics based approach for modelling suspensions*, J. Rheol. **49**, 401 (2005).

[11] I. Pagonabarraga, D. Frenkel, *Dissipative particle dynamics for interacting systems*, J. Chem. Phys. **115**, 5015 (2001).

[12] I.V. Pivkin, G.E. Karniadakis, *Coarse-graining limits in open and wall-bounded dissipative particle dynamics systems*, J. Chem. Phys. **124**, 184101 (2006).

[13] C.P. Lowe, *An alternative approach to dissipative particle dynamics*, Europhys. Lett. **47**, 145 (1999).

[14] B. Hafskjold, C.C. Liew, W. Shinoda, *Can such long time steps really be used in dissipative particle dynamics simulations?*, Mol. Simul. **30**, 879 (2004).

[15] M. Ndao, J. Devemy, A. Ghoufi, P. Malfreyt, *Coarse-Graining the Liquid–Liquid Interfaces with the MARTINI Force Field: How Is the Interfacial Tension Reproduced?*, J. Chem. Theory Comput. **11**, 3818 (2015).

[16] K.P. Travis, M. Bankhead, K. Good, S.L. Owens, *New parametrization method for dissipative particle dynamics*, J. Chem. Phys. **127**, 014109 (2007).

[17] D.A. McQuarrie, *Statistical Mechanics* (Harper Collins, New York, 1976).

[18] A. Maiti, S. McGrother, *Bead–bead interaction parameters in dissipative particle dynamics: Relation to bead-size, solubility parameter, and surface tension*, J. Chem. Phys. **120**, 1594 (2004).

[19] J.A. Beattie, *Methods for the Thermodynamic Correlation of High Pressure Gas Equilibria with the Properties of Pure Gases*, Chem. Rev. (Washington D.C.) **18**, 359 (1936).

[20] J.H. Hildebrand, R.L. Scott, *The Solubility of non-electrolytes*, 3rd Ed. (Reinhold, New York, 1950).

[21] J.H. Hildebrand, G.R. Negishi, *Solubility XV. Solubility of liquid and solid Stannic Iodide in Silicon Tetrachloride*, JACS, 59, 339-341 (1937).

[22] L.D. Gelb, E.A. Müller, *Location of phase equilibria by temperature-quench molecular dynamics simulations*, Fluid Phase Equilib. **203**, 1 (2002).

Karl Travis is Reader in Computational Physics and Nuclear Waste Disposal and leads the Deep Borehole Disposal (DBD) Research Group at the University of Sheffield. He is a Fellow of the Royal Society of Chemistry (RSC) and Chairs the RSC's Statistical Mechanics and Thermodynamics interest group. He has over 19 years of experience in computational modelling including 14 in the area of nuclear waste management and disposal. He has authored over 80 scientific papers and reports. Current interests include: non-equilibrium statistical mechanics and fluid mechanics.